Cl^- Channel Inhibitors of the Arylaminobenzoate Type Act as Photosystem II Herbicides: A Functional and Structural Study†

Arno Bock,‡ Anja Krieger-Liszkay,‡ Igor Beitia Ortiz de Zarate,‡ and Gerald Schönknecht*,§,||

Institut für Biologie II, Biochemie der Pflanzen, Universität Freiburg, Schänzlestrasse 1, 79104 Freiburg, Germany, and Lehrstuhl Botanik I, Universität Würzburg, Julius-von-Sachs-Platz 2, 97082 Würzburg, Germany

Received September 14, 2000; Revised Manuscript Received January 16, 2001

ABSTRACT: The Cl^- channel blocker NPPB (5-nitro-2-(3-phenylpropylamino) benzoic acid) inhibited photosynthetic oxygen evolution of isolated thylakoid membranes in a pH-dependent manner with a K_i of about 2 μM at pH 6. Applying different electron acceptors, taking electrons either directly from photosystem II (PS II) or photosystem I (PS I), the site of inhibition was localized within PS II. Measurements of fluorescence induction kinetics and thermoluminescence suggest that the binding of NPPB to the Q_B binding site of PS II is similar to the herbicide DCMU (3-(3,4-dichlorophenyl)-1,1-dimethylurea). The effects of different arylaminobenzoate derivatives and other Cl^- channel inhibitors on photosynthetic electron transport were investigated. The structure−activity relationship of the inhibitory effect on PS II shows interesting parallels to the one observed for the arylaminobenzoate block of mammalian Cl^- channels. A molecular modeling approach was used to fit NPPB into the Q_B binding site and to identify possible molecular interactions between NPPB and the amino acid residues of the binding site in PS II. Taken together, these data give a detailed molecular picture of the mechanism of NPPB binding.

Compounds that block ion channels are important tools for characterizing the behavior and physiological function of ion channels. A few cation channel inhibitors have established specificity and well-understood blocking mechanisms (*1*), but there is less detailed knowledge of anion channel blockers. An anion channel blocker widely used in plant (*2*) and animal cells (*3*) is the arylaminobenzoate NPPB (5-nitro-2-(3-phenylpropylamino)-benzoic acid).[1] NPPB was discovered by comparing the structure−activity relationship of 219 arylaminobenzoate derivatives concerning their ability to block Cl^- fluxes across the basolateral membrane of the thick ascending limb of the loop of Henle (*3*). In this system, the Cl^- conductance is inhibited with a K_i of 80 nM (*3*). A few other Cl^- transporters in animal cells show a comparable high affinity for NPPB (*4*, *5*). Other types of Cl^- channels such as CFTR (*6*), ClC type Cl^- channels, and band 3 in erythrocytes require higher concentrations ($\geq$100 μM) for inhibition, and unspecific inhibition by higher NPPB concentrations was reported for different cation channels and even soluble enzymes (*7*). In different plant cells, plasma membrane anion channels are blocked by NPPB with a K_i between 4 and 7 μM (*2*, *8*). Whereas the molecular nature of many low affinity NPPB-binding proteins is known, none of the high affinity NPPB-binding Cl^- channels have been cloned and sequenced so far. This lack of knowledge of the molecular nature of high affinity NPPB binding sites has hampered a detailed molecular analysis of the mechanism of NPPB binding.

Looking for a high-affinity ligand for the Cl^- channel of the thylakoid membrane (*9*, *10*), we observed that photosynthetic electron transport was inhibited by arylaminobenzoates. Since the molecular nature of the membrane proteins of the thylakoid membrane is well-established and three-dimensional structures are known for some membrane protein complexes, the photosynthetic membrane is a good model system to study the molecular mechanism of NPPB binding. The binding of herbicides to the photosynthetic membrane was extensively studied, and the molecular details of the structure of some binding sites were characterized (*11*, *12*). One of the best-investigated herbicide classes are urea herbicides such as DCMU (diuron) affecting the acceptor side of PS II. They bind to the D1 protein subunit of PS II, competing with quinone for binding to the Q_B site, and therefore inhibit the electron transport from the primary quinone acceptor Q_A to the secondary quinone acceptor Q_B. For the reaction center of *Rhodopseudomonas viridis*, which is highly homologous to the D1 protein, the binding of herbicides to the Q_B site was explored in detail by X-ray crystallography (*13*−*15*).

In the present study, we investigated the effect of several arylaminobenzoate derivatives, especially NPPB, and some other Cl^- channel inhibitors on the photosynthetic electron transport chain. We measured photosynthetic oxygen evolution, fluorescence induction kinetics (*16*, *17*), and thermolu-

† Support by the Deutsche Forschungsgemeinschaft (SFB 176, TP B11, and Li 883/3-2).

* To whom correspondence should be addressed: Telephone: +1 (405) 744 5549. Fax: +1 (405) 744 7074. E-mail: schoenk@okstate.edu.

‡ Universität Freiburg.

§ Universität Würzburg.

|| Present address: Oklahoma State University, Department of Botany, 104 Life Sciences East, Stillwater, OK 74078-3013

[1] Abbreviations: DCBQ, 2,5-dichloro-*p*-benzoquinone; DCMU, 3-(3,4-dichlorophenyl)-1,1-dimethylurea; DIDS, 4,4′-diisothiocyanatostilben-2,2′-disulfonate; ferricyanide, potassium hexacyanoferrate(III); NPPB, 5-nitro-2-(3-phenylpropylamino) benzoic acid; PS I, photosystem I; PS II, photosystem II; Q_A, primary electron acceptor; Q_B, secondary electron acceptor; $S_0 - S_4$, oxidation states of the manganese cluster of the water splitting complex; SITS, 4-acetamido-4′-isothiocyanatostilben-2,2′-disulfonate.

10.1021/bi002167a CCC: $20.00
Published on Web 02/22/2001

minescence curves (*18*, *19*) to localize the NPPB binding site. We determined the structure−activity relationship of different arylaminobenzoate derivatives. Finally, we applied molecular modeling to characterize possible molecular interactions between NPPB and amino acid residues of the binding site.

MATERIALS AND METHODS

Thylakoid membranes were isolated from spinach (*Spinacia oleracea*) or pea (*Pisum sativum*) leaves according to Polle and Junge (*20*). The chlorophyll concentration was determined according to Arnon (*21*). Oxygen evolution was measured with a Clark-type electrode (Bachhofer, Germany) at saturating white light (4000 μmol quanta m^{-2} s^{-1}), in 300 mM sucrose, 20 mM KCl, 10 mM $MgCl_2$, 30 mM buffer (MES pH 6.0−6.5, MOPS pH 6.8−7.6, tricine pH > 7.6) with a chlorophyll concentration of 20 μM and 1 μM nigericin as uncoupler. Ferricyanide (2 mM) or DCBQ (500 μM) was used as electron acceptor.

The Cl^- channel blockers DIDS and SITS (nos. 26 and 27 in Table 1) were purchased from Sigma, the other inhibitors were synthesized as described by Wangemann et al. (*3*). The Cl^- channel blockers, DCBQ and nigericin were dissolved in ethanol or DMSO. The final solute concentration was kept below 1.0% in the assay, a concentration that was shown by control experiments not to affect photosynthetic oxygen evolution by itself.

Fluorescence induction curves were measured at pH 6.0 with a PAM chlorophyll fluorometer (Walz, Effeltrich, Germany) using a light intensity of 170 μmol quanta m^{-2} s^{-1} and a chlorophyll concentration of 30 μg/mL. F_0 was determined with a measuring light with a pulse frequency of 1.6 kHz automatically switched to 100 kHz upon the onset of actinic illumination.

Thermoluminescence measurements were performed at pH 7.5 with an apparatus as described by Demeter and Vass (*22*). Thermoluminescence was charged by giving a single turnover flash at −15 °C and was recorded during heating to 70 °C at a heating rate of 20 °C/min. The samples contained a chlorophyll concentration of 30 μg/mL; 30% glycerol was added as cryoprotectant. Fresh formate was obtained by adding NaOH to formic acid.

Data fitting (nonlinear regression analysis) was done with Grafit (Erithacus Software, London, U.K.) using a least-squares fit routine based on the Marquardt algorithm. For molecular modeling, the program Insight II (Molecular Simulations Inc., Munich, Germany) was used. Using the stereoviewing facility of Insight II, NPPB and other inhibitors were manually placed into the Q_B binding pocket according to the quinone position (*15*). Afterward, energy minimization and dynamics were performed using a consistent valence force field, where partial charges and potentials were assigned. Dynamics were run with 50 000 steps of 1 fs each step.

RESULTS

As shown in Figure 1, NPPB inhibited the photosynthetic oxygen evolution of isolated thylakoid membranes. The concentration dependence was identical for thylakoids from pea and spinach. For a quantitative analysis, we assumed a simple Michaelis−Menten type of inhibitor enzyme interaction with a single noncooperative binding site. This results in the following equation:

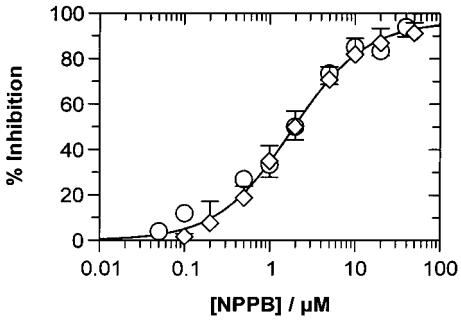

FIGURE 1: Effect of NPPB on photosynthetic oxygen evolution of isolated thylakoid membranes from pea (circles) and spinach (diamonds). As an electron acceptor, either ferricyanide (2 mM) or DCBQ (500 μM) was used. The maximum rate of oxygen evolution at pH 6.0 was 199 μmol of O_2 mg^{-1} h^{-1} in the presence of DCBQ and 145 μmol of O_2 mg^{-1} h^{-1} in the presence of ferricyanide. Oxygen evolution rates in the absence of NPPB were set to 100%, and the percentage of inhibition was plotted as mean ± SD as a function of the NPPB concentration. Since data sets measured with different electron acceptors did not differ significantly, the data were pooled for pea ($n = 4$, negative error bars) and spinach thylakoids ($n = 7$, positive error bars), respectively. The solid line shows the raw data fitted by eq 1, resulting in a $K_i = 1.8 \pm 0.1$ μM and Max = 96.4 ± 1.4%.

$$\mathrm{Inh} = \frac{\mathrm{Max[NPPB]}}{K_i + \mathrm{[NPPB]}} \quad (1)$$

where Inh is the inhibition of photosynthetic oxygen evolution in percent (*Y* axis of Figure 1), [NPPB] is the applied inhibitor concentration (*X* axis of Figure 1), Max is the theoretical maximum inhibition, and K_i is the concentration where half of the binding sites are occupied, reflecting the affinity between the enzyme and the inhibitor. The nonlinear regression analysis shown in Figure 1 resulted in a K_i value of 1.8 μM indicating a high-affinity binding of NPPB. It is worth mentioning that the second parameter determined by fitting, Max, which is expected to be 100% at complete inhibition, within error limits came close to the theoretical value of 100%. This is a good indication that the model of a simple binding isotherm formulated by eq 1 correctly describes our data.

It is most likely that the observed inhibition of photosynthetic oxygen evolution in the presence of NPPB is due to a blockage of photosynthetic electron transport. To test where NPPB is binding, we applied different electron acceptors taking electrons either directly from PS II or from PS I. The site of inhibition was localized within PS II, since O_2 evolution was blocked by NPPB with all electron acceptors tested (Figure 1). Moreover, oxygen evolution of PS II-enriched membrane fragments isolated according to Berthold et al. (*23*) was inhibited by NPPB as well, corroborating a binding of NPPB to PS II.

To further investigate the binding of NPPB to PS II, the pH dependence of K_i values in the pH range 5.5 to 8.0 was determined. As shown in Figure 2, for thylakoid membranes from pea and spinach, K_i values increased with increasing pH values. For a quantitative analysis, we assumed a simple titration, described by the following equation

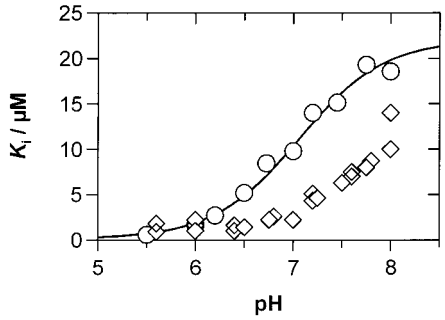

FIGURE 2: The pH dependence of inhibition of photosynthetic oxygen evolution by NPPB for pea thylakoids (circles) and spinach thylakoids (diamonds). Measurements were performed as described in Figure 1. The maximum rate of oxygen evolution at pH 6.0, 6.5, 7.0, 7.5, 8.0 was 199, 246, 327, 303, and 252 μmol of O_2 mg^{-1} h^{-1} in the presence of DCBQ, respectively, and 145, 188, 195, 164, and 130 μmol of O_2 mg^{-1} h^{-1} in the presence of ferricyanide, respectively. The K_i values estimated by data fitting as shown in Figure 1 for each pH value are plotted as a function of pH. For pea thylakoids, mean values from six experiments are given. Three experiments were performed with spinach thylakoids. The raw data from pea thylakoids were fitted by eq 2 (solid line), resulting in $K_a = 0.1 \pm 0.9$ μM, $K_b = 22.1 \pm 1.7$ μM, p$K = 7.1 \pm 0.1$.

$$K_i = \frac{K_a + K_b 10^{(pH - pK)}}{10^{(pH - pK)} + 1} \quad (2)$$

where K_i gives the affinity between the enzyme and the inhibitor (Y axis of Figure 2), pH is the applied pH (X axis of Figure 2), K_a is the minimum K_i value at very acidic conditions, K_b is the maximum K_i value at very basic conditions, and pK gives the pH value at which every second proton binding site is protonated. The nonlinear regression analysis, shown in Figure 2, resulted in a pK value of 7.1 and a maximum K_i value of $K_b = 22$ μM at basic pH values. The minimum K_i value K_a at acidic pH values could not reliably be determined but is probably below 1 μM. With the data from spinach thylakoids, this three-parameter fit could not be performed, since the existing data points do not indicate the region of steepest slope (turning point of titration curve). Since photosynthetic oxygen evolution is inhibited at pH values above 8.0, no quantification of the NPPB-dependent inhibition is possible above this value. Figure 2 shows that the pK value approaching pH 8.0 for spinach thylakoids is nearly one pH unit higher than for pea thylakoids.

For a more detailed localization of the NPPB binding site within PS II, fluorescence induction curves (*16*, *24*) were recorded in the presence and in the absence of NPPB (Figure 3). In the absence of an inhibitor, the classical three-phasic fluorescence rise kinetics were observed (*16*). In the presence of NPPB, the fluorescence induction was accelerated and the maximal fluorescence level was slightly quenched. The same fast induction kinetics are obtained in the presence of DCMU, a well-known inhibitor of the acceptor side of PS II (*16*). The similar effect of DCMU and NPPB on fluorescence induction curves (Figure 3) indicates that NPPB is binding to the acceptor side of PS II, probably at the Q_B-binding site of the D1 subunit of PS II where DCMU is acting.

To further characterize the inhibitory effect of NPPB, thermoluminescence measurements were performed (*18*, *19*). Figure 4 shows thermoluminescence bands of spinach

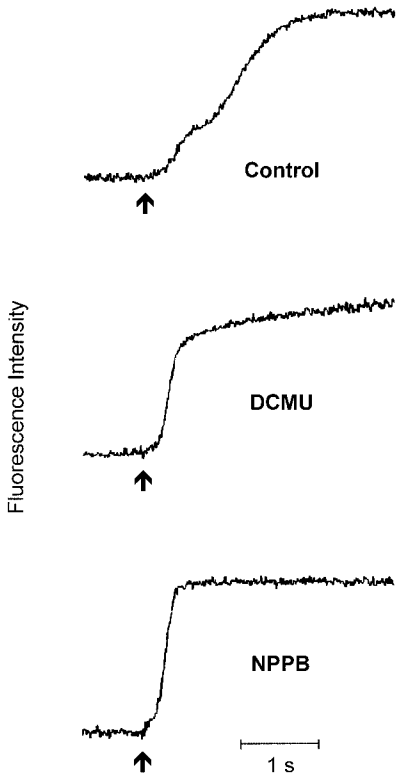

FIGURE 3: Fluorescence induction curves of spinach thylakoid membranes without an inhibitor (control) and in the presence of 1.8 μM NPPB or 1 μM DCMU, starting from the F_o level. The arrow indicates the onset of actinic illumination (170 μmol quanta m^{-2} s^{-1}).

thylakoid membranes after one saturating single turnover flash in the absence of inhibitors and in the presence of NPPB, DCMU, or formate. In thermoluminescence, the emitted light originates from charge recombination of trapped charge pairs. The charge pairs can be identified by their emission temperatures, which strongly depend on the redox potentials of the charge pairs involved. The B and the Q-band are most important thermoluminescence bands for investigating inhibitory effects of herbicides on the electron transfer from Q_A to Q_B in PS II. The recombination of the S_2 or S_3 states of the manganese cluster of the oxygen-evolving complex at the donor side of PS II with the semiquinone Q_B^- at the acceptor side yields the B band at approximately 30 °C. A $S_2Q_A^-$ recombination results in the Q-band at approximately 0−5 °C (*18*). Without any addition (control), the B band had a maximum emission temperature at about 30 °C. In the presence of NPPB or DCMU, the thermoluminescence emission was shifted to a lower temperature of about −2 °C (NPPB) or 2 °C (DCMU), which indicates a blockage of electron transfer from Q_A to Q_B. Formate also acts as an inhibitor on the acceptor side of PS II, but it competes with HCO_3^- at the non-heme iron-binding site (*25*). In the presence of formate, the B band emission temperature is increased from approximately 30 °C to approximately 38 °C (Figure 4, bottom). Additionally, a small shoulder at about 48 °C might reflect a C band, which is assigned to a $Tyr_D^+Q_A^-$ recombination (*26*).

In addition, thermoluminescence intensities were measured as a function of the number of excitation flashes in the presence and absence of NPPB (data not shown). In the absence of NPPB, the B-band oscillates with a period of four

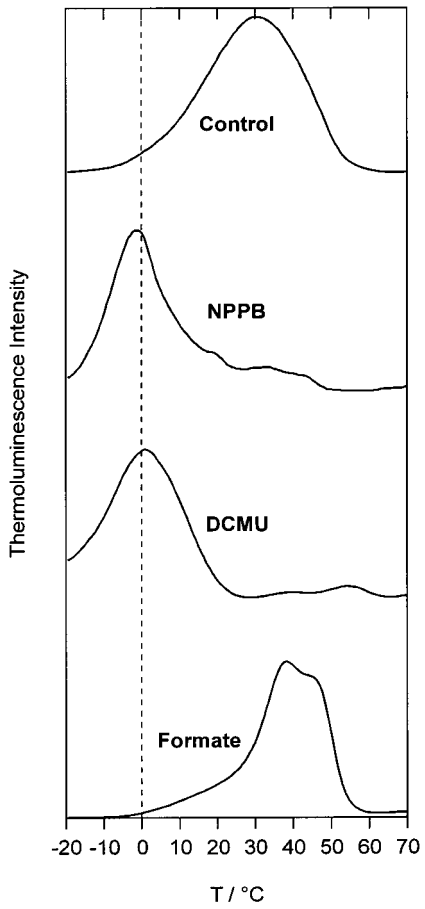

FIGURE 4: Thermoluminescence measurements of spinach thylakoid membranes with no addition (control), in the presence of 10 μM NPPB, 10 μM DCMU, or 20 mM formate, respectively.

representing an active electron transport chain. In the presence of NPPB, no such oscillation was observed as expected for a Q-band indicating blocked electron transfer between Q_A and Q_B. The thermoluminescence data provide strong evidence for a similar mode of action of NPPB and DCMU at the acceptor side of PS II.

We evaluated the structure−function relationship of various arylaminobenzoate derivatives and other Cl^- channel blockers by comparing their effects on oxygen evolution. For each substance that caused a significant inhibition of photosynthetic electron transport, measurements were performed with ferricyanide as well as with DCBQ. In each case, O_2 evolution was inhibited to the same degree with both electron acceptors, indicating that inhibition was due to binding to the acceptor side of PS II for all inhibitors tested. As a quantitative basis for a discussion of the structure−activity relationship, K_i values for the different substances (summarized in Table 1) were determined as in Figure 1.

DISCUSSION

The results of the present study show that several Cl^- channel inhibitors of the arylaminobenzoate type are able to inhibit the electron transfer in PS II at low concentrations and, therefore, to act as effective herbicides. Although the experiments presented here were performed with isolated thylakoids, NPPB being rather lipophilic (*3*) also blocks photosynthetic electron transport in intact plant cells. Obviously, in green plant cells NPPB is not specific for plasma membrane anion channels. The affinity of PS II for NPPB ($K_i = 1.8\ \mu$M) is even higher than the affinity of plant plasma membrane Cl^- channels (4−7 μM) (*2*, *8*). Therefore, effects of NPPB on intact cells or whole plants must be interpreted with great care and do not necessarily indicate the involvement of plasma membrane anion channels.

The data presented in Figures 3 and 4 indicate that NPPB, comparable to DCMU, blocks electron transfer from Q_A to Q_B at the electron acceptor side of PS II. An inhibition of photosynthetic water splitting at the donor side of PS II as observed in the presence of so-called ADRY reagents (*a*cceleration of the *d*eactivation *r*eactions of the water-splitting enzyme system *Y*) can be excluded. These ADRY reagents significantly diminish the intensity of thermoluminescence bands (*27*), and the initial, fast phase of fluorescence induction curves is suppressed (*24*, *28*). None of those effects was observed in the presence of NPPB.

Another possible candidate for NPPB binding could be the non-heme iron at the acceptor side of PS II. In active PS II, one coordination site of this non-heme iron is occupied by bicarbonate. NPPB containing a carboxyl group with a p*K* value of 4.5 (*3*, *5*) was deprotonated under our measuring conditions and thus might have competed with bicarbonate. However, the thermoluminescence curve in the presence of NPPB was clearly different from that in the presence of formate (Figure 4), which effectively competes with bicarbonate (*25*, *29*), indicating that NPPB did not act as a ligand for the non-heme iron by replacing bicarbonate.

The inhibitory effect of NPPB on photosynthetic oxygen evolution decreases with increasing pH values (Figure 2) with p*K* values of 7.1 and 8.0 for pea and spinach, respectively. The p*K* of NPPB itself is about 4.5 (*3*, *5*) so that its carboxy group is deprotonated at all pH values used here. Moreover, a protonation/deprotonation of NPPB would hardly show a significant species-specific difference. Thus, a protonation/deprotonation of one or more amino acid residues at the acceptor side of PS II likely affects NPPB binding. A comparable species-specific difference between p*K* values was reported for the kinetics of the pH-dependent electron transfer from Q_A to Q_B (*30*, *31*). The p*K* value of the inhibition of oxygen evolution by a phenolic herbicide for spinach was the same as reported here (*32*). The only amino acid with a p*K* in the range between pH 7 and pH 8 is histidine with a p*K* value between pH 4 to pH 8 depending on the intramolecular environment. Possible candidates are His D1 215 and/or His D1 272 located at the top of the Q_B binding site (*33*) (see below).

A pH-dependence between pH 7 and pH 8 is well within the physiological range. The pH value in the chloroplast stroma of darkened leaves is pH 7.5 to pH 8.0. Upon illumination, the chloroplast stroma is alkalized by 0.1 to 0.6 pH units (*34*, *35*). The titration curves for both pea and spinach are steep (Figure 2) in the pH range where light-dependent pH changes in the stroma occur.

The data summarized in Table 1 identify which structural elements of arylaminobenzoate derivatives are required to block electron transport in PS II. The negatively charged carboxylate group of the benzoate moiety seems to be of utmost importance for the inhibitory effect. Substitution of the carboxylate group of NPPB (no. 13, numbers refer to numbering in Table 1) with a sulfonyl group

Table 1: Inhibition of Photosynthetic Oxygen Evolution by Cl⁻ Channel Blockers[c]

No.	Structure	Name	K_i value [a]	K_i kidney [b]
1	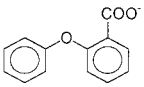	2-Phenoxybenzoate	No inhibition	> 100 μM
2	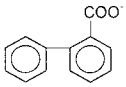	Biphenyl-2-carboxylate	> 100 μM	> 100 μM
3	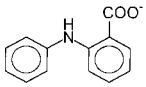	Diphenylamine-2-carboxylate (DPC)	90±1.7 μM	26 μM
4	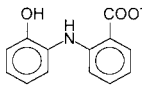	2'-Hydroxydiphenylamine-2-carboxylate	> 100 μM	80 μM
5	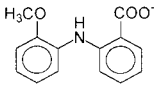	2'-Methoxydiphenylamine-2-carboxylate	> 100 μM	75 μM
6	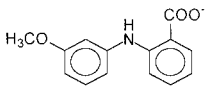	3'-Methoxydiphenylamine-2-carboxylate	~ 100 μM	~ 100 μM
7	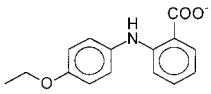	4'-Ethoxydiphenylamine-2-carboxylate	> 100 μM	48 μM
8	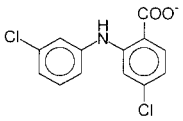	3',5-Dichlorodiphenylamine-2-carboxylate (DCDPC)	21.8±1.6 μM	16 μM
9	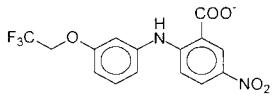	2-[3-(2,2,2-Trifluorethoxy)]-phenylamino-5-nitrobenzoate	5.8±0.5 μM	n.t.
10	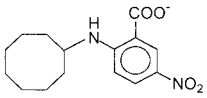	2-Cyclooctylamino-5-nitrobenzoate	1.4±0.1 μM	5.5 μM
11	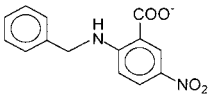	2-Benzylamino-5-nitrobenzoate (NPMB)	12.8±0.9 μM	30 μM
12	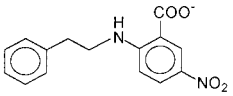	5-Nitro-2-(2-phenylethyl-amino)-benzoate (NPEB)	5.2±0.5 μM	0.3 μM
13	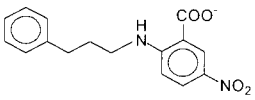	5-Nitro-2-(3-phenylpropyl-amino)-benzoate (NPPB)	1.8±0.1 μM	80 nM
14	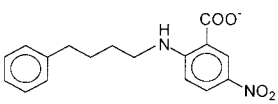	5-Nitro-2-(4-phenylbutyl-amino)-benzoate (NPBB)	1.2±0.1 μM	1.8 μM

Table 1: (Continued)

No.	Structure	Name	K_i value [a]	K_i kidney [b]
15	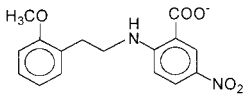	2-(2-(2-Methoxyphenyl)-ethylamino)-5-nitrobenzoate	4.7±0.6 μM	60 μM
16	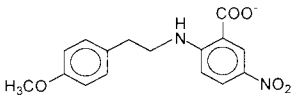	2-(2-(4-Methoxyphenyl)-ethylamino)-5-nitrobenzoate	3.4±0.35 μM	~ 100 μM
17	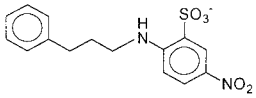	5-Nitro-2-(3-phenylpropylamino)-benzenesufonate (NPPS)	55±2.4 μM	n.t.
18	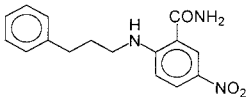	5-Nitro-2-(3-phenylpropyl-amino)-benzamide	~ 200 μM	n.t.
19	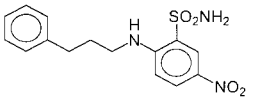	5-Nitro-2-(3-phenylpropyl-amino)-benzenesulfonamide	~ 300 μM	n.t.
20	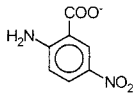	2-Amino-5-nitrobenzoate	No inhibition	n.t.
21	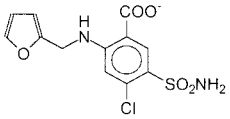	4-Chloro-N-furfuryl-5-sulfamoylanthranilic acid (Furosemide)	> 100 μM	n.t.
22	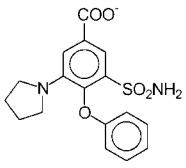	4-Phenoxy-3-(1-pyrrolidinyl)-5-sulfamoylbenzoate (Piretanide)	> 100 μM	n.t.
23	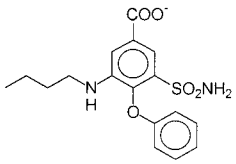	3-Butylamino-4-phenoxy-5-sulfamoylbenzoate (Bumetanide)	No inhibition	n.t.
24	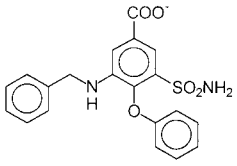	3-Benzylamino-4-phenoxy-5-sulfamoylbenzoate (Benzmetanide)	No inhibition	n.t.
25	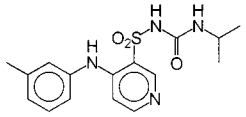	N-[[(1-methylethyl)amino] carbonyl]-4-[(3-methylphenyl] amino]-3-pyridinesulfonamide (Torasemide)	> 100 μM	34 μM
26	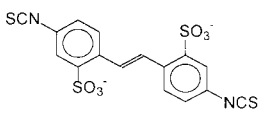	4,4'-Diisothiocyanatostilben-2,2'-disulfonate (DIDS)	No inhibition	n.t.

Table 1: (Continued)

No.	Structure	Name	K_i value [a]	K_i kidney [b]
27	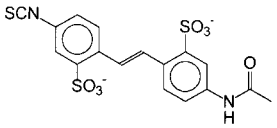	4-Acetamido-4'-isothiocyanatostilben-2,2'-disulfonate (SITS)	No inhibition	n.t.
28	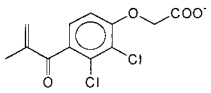	(2,3-Dichloro-4-(2-methylene-butyryl)-phenoxy)-acetate (Ethacrynic acid)	> 100 μM	n.t.

[a] Where K_i values ± SE are given, the binding affinity was determined by nonlinear regression analysis with complete concentration dependencies as shown in Figure 1. For those chloride channel blockers with a lower affinity, an approximate K_i was estimated or it is indicated that the K_i is larger than 100 μM. "No inhibition" means that within the testable concentration range no significant inhibition of photosynthetic oxygen evolution could be detected. [b] For comparison, K_i values from the publication discovering NPPB as Cl^- channel blocker in kidney cells (*3*) are given; n.t. = not tested. The numbering refers to the numbers in the text. [c] Oxygen evolution was measured at pH 6.0 with either ferricyanide (2 mM) or DCBQ (500 μM) as electron acceptor yielding maximum rates of 145 μmol of O_2 mg^{-1} h^{-1} or 199 μmol of O_2 mg^{-1} h^{-1}, respectively.

(NPPS or no. 17) increased the K_i value more than 25-fold even though the negative charge is conserved. Replacing the carboxylate group by an uncharged benzamid moiety (no. 18) increased the K_i value by more than 2 orders of magnitude. Similarly, substitution by an uncharged sulfamoyl group (no. 19) nearly abolished the inhibitory effect on PS II.

Another essential element for arylaminobenzoate binding to PS II seems to be an additional negative partial charge in para or meta position to the carboxylate group. All potent inhibitors have either $-NO_2$ in the 5-position or -Cl in the 4-position of the benzoate moiety. Whereas no. 4 to no. 7 lack an additional electronegative group and had little inhibitory effect, no. 9 with $-NO_2$ in 5-position, displayed a high affinity ($K_i = 6$ μM). Although the different substituents at the second ring might also contribute to the different affinities (see below), the $-NO_2$ group is probably most important. Additional electronegative groups in 4-position of the benzoate moiety (and on the phenyl ring) increase the binding affinity more than 4-fold (no. 3 as compared to no. 8).

The secondary amino group represents another functionally important component of the molecule. As compared to no. 1 and no. 2, no. 3 (DPC) has a higher affinity for PS II due to the amino group between the two phenyl rings. This secondary amino group carries a partial positive charge. The stabilization of this positive partial charge by electronegative groups on the second ring might contribute to the good affinity of no. 8 and no. 9.

The secondary amino group connects the nitrobenzoate moiety to a hydrophobic side chain. This side chain is indispensable for inhibition of photosynthetic oxygen evolution, since its removal results in an inactive substance (no. 20). Within the hydrophobic side chain, an increase in the spacing between the secondary amino group and the second ring (no. 11 to no. 14) increases the inhibitory potency remarkably. As compared to $K_i = 13$ μM with a $-CH_2-$ spacer (no. 11, NPMB), the affinity increased by 1 order of magnitude with a $-(CH_2)_4-$ spacer (no. 14, NPBB). From no. 10, it is apparent that a cyclooctyl ring can substitute for a $-C_4H_8-$ spacer plus phenyl ring, since no. 10 has nearly the same high affinity as no. 14 (NPBB). The inhibitory effect on PS II seems to depend on a relative bulky hydrophobic side chain. With a $-(CH_2)_4-$ spacer separating the secondary amino group from the second ring as in NPEB (no. 12), additional groups on the second ring like in no. 15 and no. 16 seem to have little effect on the binding affinity, although the affinity increases with the size of the substituent bound to the secondary amino group.

Summarizing, four characteristic elements of arylaminobenzoates are necessary for binding to the Q_B binding niche of PS II: (i) the anionic carboxylate group; (ii) the negative partial charge in meta (or para) position to the carboxylate group; (iii) the amino "bridge" carrying a positive partial charge; and (iv) the bulky hydrophobic side chain.

On the basis of these characteristic elements, one can understand why photosynthetic electron transport is inhibited by NPPB but not by other established drugs binding to Cl^- transporters (nos. 20 to 28). Furosemid (no. 21) in principle has all the characteristic elements mentioned above, and it is probably the large sulfamoyl group in meta position to the carboxylate group that causes some sterical hindrance preventing binding. All other sulfamoylbenzoates (no. 22 to no. 24) also carry this sulfamoyl group and in contrast to furosemide do not display all the characteristic elements mentioned above. Torasemide (no. 25), DIDS (no. 26), SITS (no. 27), and ethacrynic acid (no. 28) have structures completely different from those of arylaminobenzoates.

As compared to the original study discovering NPPB as a potent Cl^- channel inhibitor (*3*), there is a very significant degree of correspondence in the structure−activity relationship (Table 1). The same four sites of arylaminobenzoates interact with the Cl^- channel in mammalian kidney: (i) an anionic carboxylate group; (ii) a negative partial charge on a nitro substituent in 5-position to the carboxylate; (iii) an amino "bridge" that carries a positive partial charge; and (iv) a hydrophobic site represented by a phenyl, cycloalkyl, pyrrol, or pyrrolidino ring (*3*). Nevertheless, some differences exist: as compared to PS II, the affinity of the mammalian kidney Cl^- channel for NPPB is higher ($K_i = 80$ nM). NPBB (no. 14), for example, was more effective than NPPB (no. 13) in PS II, whereas it is 20-fold less effective in kidney Cl^- channels (*3*). Because of the high overall agreement in the structure−activity relationship, it is tempting to speculate

that the binding sites for NPPB in these two different systems, kidney Cl^- channels and PS II, share a common molecular architecture.

For the cAMP-dependent Cl^- current in guinea pig ventricular myocytes, it was reported that increasing the length of the carbon chain between the benzoate and the second ring increased the potency of the drug block (*5*). K_i values decreased from 47 μM for NPMP (no. 11) to 17 μM for NPEB (no. 12) and to 4 μM for NPPB. Moreover a pH-dependence was observed with decreasing NPPB affinities at alkaline pH (*5*). Both observations are comparable to the results presented here. In a structure−activity study with the CFTR Cl^- channel, it was observed that the K_i value increases from 166 to 815 μM upon removal of the 5-nitro group from NPPB (*6*).

To further investigate the binding of NPPB to PS II, we applied molecular modeling to fit NPPB into the Q_B binding site. For PS II that binds NPPB, no structure exists with a high enough resolution to assign the binding of herbicides to the Q_B site. However, the structure of the D1 and D2 subunits of PS II strongly matches the structure of the L and M subunits of the bacterial photosynthetic reaction center (*33*, *36*), which are investigated up to a resolution of 2.3 Å for *Rhodopseudomonas viridis* (*13*, *15*, *37*). Especially at the Q_B binding site, some amino acids are conserved from purple bacteria to cyanobacteria and higher plants. Whereas the *R. viridis* wild type is insensitive to DCMU, the T4 mutant (Tyr L222 → Phe) is sensitive to DCMU (*38*). NPPB inhibits the Q_A to Q_B electron transfer in the T4 mutant as we could show by measuring the $P^+Q_B^-$ or $P^+Q_A^-$ recombination kinetics, respectively, by flash-induced absorption changes in the near infrared (data not shown). Therefore, we used the structure of the T4 mutant as the modeling basis. X-ray crystallographic analysis (*14*, *39*) showed that the different herbicide affinities of the wild-type and the T4 mutant of the bacterial reaction center are not attributable to significant structural changes within the Q_B binding pocket. Rather, there is a conformational change at the junction of the L and M subunits (*14*, *39*), possibly due to an H bond between Tyr L222 and Asp M43 as determined by the surface complementarity approach of Sobolev et al. (*40*). This H bond cannot be established in the T4 mutant due to the mutation of Tyr L222 to Phe L222. In good agreement, energy minimization calculations for the isolated wild type L subunit resulted in nearly the same size and shape of the binding site as the simulated mutant L subunit. Once one of the ligands is modeled into the binding pocket, the extent and the shape of the pocket change within ranges of about 1 Å.

The most important feature of this modeling is to show that NPPB fits into the Q_B binding site in a similar way as the quinone does. The total potential energy of the L subunit NPPB complex as determined by molecular modeling was approximately 900 kJ/mol. A snapshot (one out of 5000 calculations) of the molecular dynamics is shown in Figure 5. NPPB fits very tightly into the Q_B binding site, and the carboxylic group of NPPB is able to build H bonds to Asn L213, Ser L223, Ile L224, and Ala L226. As compared to this, putative hydrogen bonds between Q_B and the L subunit, determined based upon the surface complementarity approach developed by Sobolev et al. (*40*), involve His L190, Ser L223, Ile L224, and Gly L225. In the model (Figure 5),

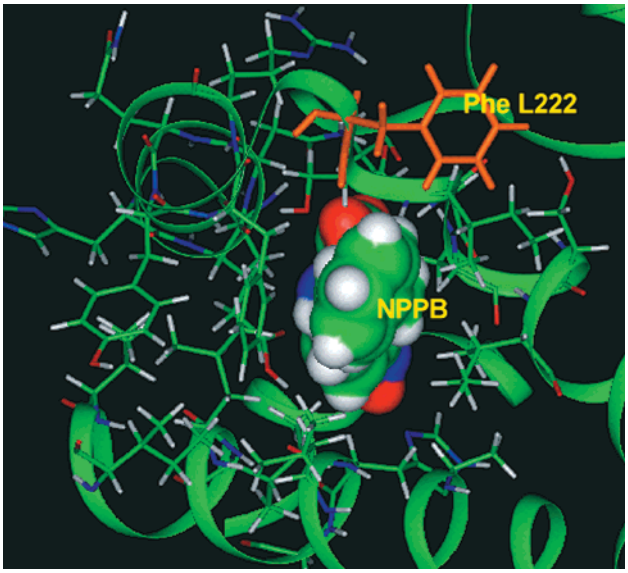

FIGURE 5: NPPB fitted into the Q_B binding pocket of the T4 mutant of *Rhodopseudomonas viridis*. The protein inhibitor complex was oriented to give a view down into the Q_B binding pocket. The ribbon indicates the backbone of the L subunit, and all amino acids with a distance of less than 7 Å from the center of NPPB are displayed.

NPPB is in close contact to His L190 (corresponding to His D1 215), whereas there is no direct contact to His L230 (corresponding to His D1 272). With respect to the observed pH dependence of NPPB binding (Figure 2), this could indicate that His D1 215 is involved. However, considering an amino acid identity between spinach and pea of 98.9% in the D1 and 96.9% in the D2 subunit, a species-specific difference of the p*K* values of about one pH unit comes as a surprise. Yet, an inspection of the few varying amino acids shows a difference in the neighborhood of His D1 215. At position D2 269, there is a histidine in spinach but a thyrosine in pea. According to current models (*41*), the amino acid at D2 269 is in direct contact to His D1 215.

In the model shown in Figure 5, the second aromatic substituent of NPPB is placed outside the binding pocket. NPEB (no. 12) was fitted into the binding site (not shown) in a similar orientation resulting in a total potential energy of about 1700 kJ/mol. Because of the reduced alkyl spacer length it was difficult to place the second aromatic substituent outside the binding pocket. Only a few positions without sterical hindrance at the edge of the binding site could be realized. This is a possible explanation for the lower affinity of NPEB (no. 12) as compared to NPPB (no. 13).

Finally, DCMU was fitted into the Q_B binding site of the T4 mutant of *R. viridis*. The total potential energy of the protein inhibitor complex was determined to be approximately 2000 kJ/mol. In the resulting model, DCMU was not able to form H bonds to the protein. The position of DCMU within the binding side obtained by molecular modeling was in good agreement to X-ray crystallographic data (*14*, *39*, *42*).

In conclusion, the present report provides evidence that arylaminobenzoate derivatives are efficient inhibitors of photosynthetic electron transfer (Figures 1 and 2) at the acceptor side of PS II (Figures 3 and 4). The structure−activity relationship (Table 1) shows which structural elements of arylaminobenzoates are important for binding and the molecular modeling shows (Figure 5) which amino acids

interact with the inhibitor. Together these data for the first time characterize a high-affinity NPPB binding site at the molecular level. The structural similarities between the compounds found to inhibit both PS II activity and Cl^- channel activity in mammalian cells strongly suggest that the molecular mode of action of arylaminobenzoates is comparable in both systems.

ACKNOWLEDGMENT

We thank W. Haehnel, B. Rosengarten (Freiburg), W. Junge, K. Lübbers (Osnabrück), and W. Henley (Stillwater) for fruitful discussions, K. Kienzler (Freiburg), M. Laubender, S. Lang, and D. Rassau (Würzburg) for skillful technical assistance, and U. Schreiber and C. Neubauer (Würzburg) for help with the fluorescence induction curves. W. Haehnel provided the computer program Insight II.

REFERENCES

1. Hille, B. (1992) *Ionic Channels of Excitable Membranes*, Sinauer Assoc. Inc., Sunderland, Massachusetts.
2. Marten, I., Zeilinger, C., Readhead, C., Al-Awqati, Q., and Hedrich, R. (1992) *EMBO J. 11*, 3569−3575.
3. Wangemann, P., Wittner, M., Di Stefano, A., Englert, H. C., Lang, H. J., Schlatter, E., and Greger, R. (1986) *Pflügers Arch. 407*, 128−141.
4. Tilmann, M., Kunzelmann, K., Fröbe, U., Cabantchik, I., Lang, H. J., Englert, H. C., and Greger, R. (1991) *Pflügers Arch. 418*, 556−563.
5. Walsh, K. B., and Wang, C. (1998) *Mol. Pharmacol. 53*, 539−546.
6. Walsh, K. B., Long, K. J., and Shen, X. (1999) *Br. J. Pharmacol. 127*, 369−376.
7. Schultz, B. D., Singh, A. K., Devor, D. C., and Bridges, R. J. (1999) *Physiol. Rev. 79*, S109−S144.
8. Schroeder, J. I., Schmidt, C., and Sheaffer, J. (1993) *Plant Cell 5*, 1831−1841.
9. Schönknecht, G., Hedrich, R., Junge, W., and Raschke, K. (1988) *Nature 336*, 589−592.
10. Pottosin, I. I., and Schönknecht, G. (1995) *J. Membr. Biol. 148*, 143−156.
11. Bowyer, J. R., Camilleri, P., and Vermaas, W.-F. J. (1991) in *Herbicides* (Baker, M. A., and Percival, M. P., Eds.) pp 27−85, Elsevier, New York.
12. van Rensen, J. J. S. (1989) in *Herbicides and Plant Metabolism* (Dodge, A. D., Ed.) pp 37−50, Cambridge University Press, Cambridge, UK.
13. Deisenhofer, J., and Michel, H. (1989) *EMBO J. 8*, 2149−2169.
14. Sinning, I. (1992) *Trends Biochem. Sci. 17*, 150−154.
15. Lancaster, C. R. D., and Michel, H. (1999) *J. Mol. Biol. 286*, 883−898.
16. Neubauer, C., and Schreiber, U. (1987) *Z. Naturforsch. 42*, 1246−1254.
17. Krause, G. H., and Weis, E. (1991) *Annu. Rev. Plant Physiol. Plant Mol. Biol. 42*, 313−349.
18. Rutherford, A. W., Crofts, A., and Inoue, Y. (1982) *Biochim. Biophys. Acta 682*, 457−465.
19. Vass, I., and Inoue, Y. (1992) in *The Phototsystems: Structure, Function, and Molecular Biology* (Barber, J., Ed.) pp 259−294, Elsevier, Amsterdam.
20. Polle, A., and Junge, W. (1986) *Biochim. Biophys. Acta 848*, 257−264.
21. Arnon, D. I. (1949) *Plant Physiol. 24*, 1−15.
22. Demeter, S., and Vass, I. (1989) *Biochim. Biophys. Acta 764*, 24−32.
23. Berthold, D. A., Babcock, G. T., and Yocum, C. F. (1981) *FEBS Lett. 134*, 231−234.
24. Schreiber, U., and Neubauer, C. (1987) *Z. Naturforsch. 42*, 1255−1264.
25. Govindjee (1993) *Z. Naturforsch. 48*, 251−258.
26. Johnson, G. N., Boussac, A., and Rutherford, A. W. (1994) *Biochim. Biophys. Acta 1184*, 85−92.
27. Renger, G., and Inoue, Y. (1983) *Biochim. Biophys. Acta 725*, 146−154.
28. Hanssum, B., Dohnt, G., and Renger, G. (1984) *Biochim. Biophys. Acta 806*, 210−220.
29. Govindjee, Nakatani, H. Y., Rutherford, A. W., and Inoue, Y. (1984) *Biochim. Biophys. Acta 766*, 416−423.
30. Robinson, H. H., and Crofts, A. (1983) in *Advances in Photosynthesis Research* (Sysbema, C., Ed.) pp 447−480, Kluwer Academic Publisher, Dordrecht, The Netherlands.
31. Eaton-Rye, J. J., Govindjee (1988) *Biochim. Biophys. Acta 935*, 248−257.
32. Nakajima, Y., Yoshida, S., Inoue, Y., and Ono, T. (1996) *J. Biol. Chem. 271*, 17383−17389.
33. Trebst, A. (1986) *Z. Naturforsch. 41*, 240−245.
34. Heineke, D., and Heldt, H. W. (1988) *Bot. Acta 101*, 45−47.
35. Laisk, A., Oja, V., Kiirats, O., Raschke, K., and Heber, U. (1989) *Planta 177*, 350−358.
36. Michel, H., and Deisenhofer, J. (1988) *Biochemistry 27*, 1−7.
37. Deisenhofer, J., Epp, O., Sinning, I., and Michel, H. (1995) *J. Mol. Biol. 246*, 429−457.
38. Sinning, I., Michel, H., Mathis, P., and Rutherford, A. W. (1989) *Biochemistry 28*, 5544−5553.
39. Sinning, I., Koepke, J., and Michel, H. (1990) in *Reaction Centers of Photosynthetic Bacteria* (Michel-Beyerle, M. E., Ed.) pp 199−208, Springer Publisher.
40. Sobolev, V., Sorokine, A., Prilusky, J., Abola, E. E., and Edelman, M. (1999) *Bioinformatics 15*, 327−332.
41. Xiong, J., Subramaniam, S., and Govindjee (1996) *Protein Sci. 5*, 2054−2073.
42. Mackay, S. P., and O'Malley, P. J. (1993) *Z. Naturforsch. 48*, 191−198.

BI002167A